<u>Title:</u> Catalytic Reduction of Dinitrogen to Ammonia using Molybdenum Porphyrin Complexes

Authors: Alexander S. Hegg, Brandon Q. Mercado, Alexander J. M. Miller, Patrick L. Holland*

<u>Abstract:</u> Porphyrin complexes are well-known in O₂ and CO₂ reduction, but their application to N₂ reduction is less developed. Here, we show that oxo and nitrido complexes of molybdenum supported by tetramesitylporphyrin (TMP) are effective precatalysts for catalytic N₂ reduction to ammonia, verified by ¹⁵N₂ labeling studies and other control experiments. Spectroscopic and electrochemical studies illuminate some relevant thermodynamic parameters, including the N–H bond dissociation free energy of (TMP)MoNH (43±2 kcal/mol). We place these results in the context of other work on homogeneous N₂ reduction catalysis.

Introduction

Industrial nitrogen fixation to ammonia (NH₃) is performed on a 182 million ton/year scale¹ and 40% of the world population depends on the increased agricultural output supported by fertilizers derived from this ammonia.² This is achieved through the Haber-Bosch Process (HBP), which combines dinitrogen (N₂) and dihydrogen (H₂) to produce NH₃. While this process is effective, the H₂ gas used in the HBP is generally derived from steam reforming of fossil fuels, which results in massive release of carbon dioxide (CO₂) – around 1.5% of global emissions annually.³⁻⁶ In addition, high temperatures are required for the HBP. It is estimated that the steam-reforming-based HBP is responsible for around 1-3% of annual global energy usage and massive amounts of CO₂.^{6,7} To improve the sustainability of NH₃ production, some experimental plants are switching

to H₂ produced via electrolysis of water driven by wind power,^{8,9} enabling the decentralization of the operation. While this method avoids the CO₂ from steam reforming, it maintains the temperature and pressure disadvantages of the HBP. An alternative is to add protons and electrons (ideally from water) in the nitrogen reduction reaction (NRR). To make this cost-competitive with the HBP, there is a need for NRR catalysts that can operate under mild conditions with high Faradaic efficiencies.^{4,5,10-12}

For homogeneous NRR, several mechanisms have been proposed, which differ in the order of e^-/H^+ addition to the nitrogen atoms. Reduction of terminally bound N_2 can proceed either through an alternating or distal mechanism. In both cases, the distal nitrogen atom is reduced first, but sequential H^+/e^- additions can either alternate between the proximal and distal nitrogen atoms (green path, Figure 1) or all H transfers can occur first to the distal N atom (blue path, Figure 1). Alternatively, a second equivalent of the metal catalyst can bind to form an N_2 -bridged dimer, which under certain conditions can split the $N\equiv N$ triple bond to form two terminal metal nitrides (red path, Figure 1).

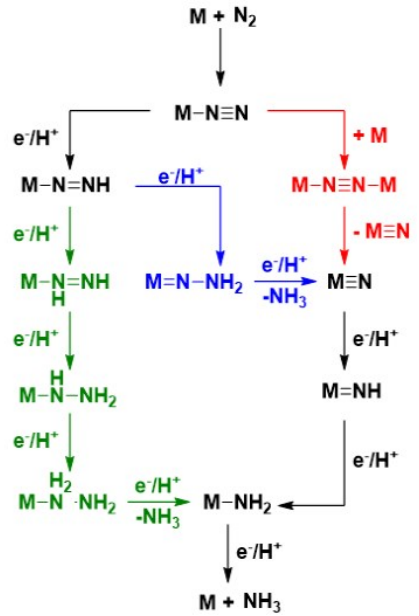


Figure 1: Pathways to NH₃ from N₂. **Red:** N₂ splitting to terminal metal nitrides. **Blue:** Reduction of the distal nitrogen to a terminal metal nitride. **Green:** Alternating reduction of the distal and proximal nitrogen atoms.¹⁴

Figure 2: A selection of N₂-to-NH₃ catalysts grouped by their proposed mechanisms. HIPT = $3,5-(2,4,6-{}^{i}\text{Pr}_{3}\text{C}_{6}\text{H}_{2})_{2}\text{C}_{6}\text{H}_{3}$.

Table 1: Reported yields and efficiencies for N₂ reduction to NH₃ catalyzed by the metal complexes shown in Figure 2 with different e⁻/H⁺ sources.

	SmI ₂ /ROH		Cp2M/Acid		Mediated eNRR		
Catalyst	Equiv.	%	Equiv.	%	Equiv.	%	References
	NH ₃ /M	Efficiency	NH ₃ /M	Efficiency	NH ₃ /M	Efficiency	
1	28	44%	12	49%	8.7	34%	21, 27, 28
2	53	88%	100	41%			21, 29
3	5.1	43%			13	51%	30, 28
4			7.6	66%			31
5	53	89%	51	84%	< 0.1	<1%	21, 32,33, 28
6	4350	91%					21

Conversion of a coordinated N2 molecule to NH3 at a homogeneous metal complex was first reported in 1975 by Chatt and coworkers. 15 Molybdenum and tungsten complexes with the formula M(PR₃)₄(N₂)₂ yielded 0.7 to 1.9 equiv. of NH₃ per M when exposed to H₂SO₄ in methanol, the electrons required for the reaction coming from the oxidation of the M⁰ precursor to M^{VI}.¹⁶ Catalysis with homogeneous metal complexes was not achieved until 2003, when Schrock and coworkers used a molybdenum dinitrogen complex with CrCp*2 and 2,6-lutidinium tetraarylborate ([LutH][BArF4]) to generate 7.6 equiv. of NH3/Mo.17 This first report was followed by other examples of terminally bound N₂ being converted catalytically to NH₃. A selection is shown in Figure 2, and several reviews give a more complete survey of these catalysts. 13,18 Most catalysts are proposed to initiate from a highly reduced terminal N2 complex and follow the distal mechanism. Initiation from a bridging N₂ complex is also possible, however, when the N₂ splitting mechanism is followed. Splitting by a homogeneous transition metal catalyst was first demonstrated by Laplaza and Cummins in 1995 wherein a tris(anilide)molybdenum(III) complex reacted with N₂ gas to generate a MoVI nitride. 19,20 Building on this work, thermal N₂ splitting to terminal metal nitrides has since been reported with a number of niobium, molybdenum, tungsten, and rhenium complexes. ²¹⁻²⁶ Among these N₂-splitting complexes, several have been reported as

NRR catalysts, and a selection of molybdenum complexes are shown in Figure 2. The catalysts are grouped by the mechanism that has been proposed, but a full mechanistic analysis has not been performed for all complexes. Ammonia yields and electron efficiencies are shown for each catalyst in Table 1.

Terminal metal nitrides are a key part of NRR cycles because they are found in both the distal and N₂-splitting mechanisms, but often the nitrides derived from N₂ reduction are too stable to be converted to ammonia. In the cases where N₂ derived metal nitrides can be functionalized to generate NH₃, highly reducing conditions are often required. ^{14,25,34,35} One way to circumvent this problem is to use concerted proton-coupled electron transfer (PCET), in which the negative charge of the electron is simultaneously balanced with a proton transfer. In the consideration of PCET to a metal nitride, the metal imido bond dissociation free energy (BDFE) can be an indication of reactivity with different H-atom donors through comparison of the imido N-H BDFE to the effective BDFE of an acid/reductant pair or to the BDFE of a PCET reagent. Metal imido complexes are generally thought to have the weakest of the N-H bonds in the path from nitride to ammonia based upon computations reported for select transition metal nitride complexes. ^{14,26,36-40} Thus, if a PCET reagent or acid/reductant pair has a weaker effective BDFE than the metal imide N-H, it suggests that the reagent will be able to perform all three PCET reactions to form ammonia. The PCET reagents that have been used for NRR include SmI₂/ROH and CoCp*₂ or CoCp₂ with strong acids. ^{21,41,42}

One class of ligands that has recently received interest in NRR is porphyrins. Metalloporphyrin complexes are active catalysts for the activation and reduction of other small molecules such as O₂ and CO₂.^{43,44} Work on electrocatalytic reduction of O₂ was inspired by cytochrome c oxidase, which uses a heme active site to bind and reduce O2 to H2O. Researchers have used this as a model to develop homogeneous porphyrin catalysts and have shown that changes to the ligand can tune the performance of the catalyst. 44-46 Metalloporphyrin complexes also catalyze the reduction of CO₂ to CO and CH₄. ⁴⁷⁻⁴⁹ The successes of metalloporphyrins in the electrocatalytic activation of CO₂ and O₂ make them interesting candidates for the six-electron, six-proton NRR. Metalloporphyrin catalyzed N₂ reduction to ammonia (and ammonia oxidation to N₂) have been studied computationally for many transition metals. 40,50 These studies examine the energy of substrate binding, and H-atom addition in the case of N₂ reduction (or H-atom removal in the case of ammonia oxidation) to identify likely candidates for catalysis. Computational studies for ammonia oxidation have experimental support in bis(ammine)ruthenium tetramesitylporphyrin, which performed catalytic ammonia oxidation using a stoichiometric H-atom abstracting reagent.⁵¹ There are also recent experimental reports of eNRR using metalloporphyrin-based catalysts loaded onto carbon paper electrodes and porphyrin-based metal-organic frameworks. Some of these catalysts achieve multiple equivalents of NH₃/metal center each hour. 52-54

As mentioned above, terminal metal nitride complexes are of interest because they are intermediates along several pathways of NRR. The synthesis of porphyrin transition metal nitrides has been studied, and these complexes have found some application in performing N-atom transfer to organic reagents,⁵⁵ but to the best of our knowledge there are no reports of nitride conversion to ammonia or catalytic N₂ reduction by homogeneous porphyrin catalysts. In this paper, we report

catalytic ammonia formation from N_2 , using nitridomolybdenum tetramesitylporphyrin $[(TMP)MoN]^{56}$ as a precatalyst. Further, we quantify the imido N-H BDFE that defines the thermodynamics for the first H-atom addition to the nitride and assess the advantages and disadvantages of this system in catalysis.

Results and Discussion

Synthesis and Characterization of Molybdenum Porphyrin Complexes

It is known that Mo complexes of tetraphenylporphyrin (TPP) and tetra-p-tolylporphyrin (TTP) give dimers with Mo-Mo multiple bonds,^{57,58} which would prevent N₂ binding and catalysis. Therefore, we studied a bulky porphyrin (tetramesitylporphyrin, TMPH₂), in which the ortho substituents on the mesityl rings block the Mo sites enough to discourage dimerization.⁵⁶ Following the method reported to give the molybdenum(II) compound (TMP)Mo,⁵⁶ we heated TMPH₂ at 210 °C with an excess of Mo(CO)₆ in decalin for 24 hours under N₂. To measure the progress of the reaction, aliquots of the reaction mixture were removed, diluted with dichloromethane, and UV-vis spectra were measured. Conversion was judged based on the disappearance of peaks associated with TMPH₂. Once the peaks of TMPH₂ were no longer visible, filtration of the cooled reaction mixture gave a purple powder in quantitative yield. The ¹H NMR spectrum for this product matches the original report for (TMP)Mo, but the presence of an axial ligand on one side is indicated by the inequivalence of the mesityl o-CH₃ signals. To resolve this discrepancy, crystals suitable for diffraction were grown from the diffusion of pentane into a concentrated toluene solution of the product at -35 °C (crystallized yield 60%). An X-ray crystal structure of the isolated product indicates that the metalated species is not (TMP)Mo as previously claimed, ⁵⁶ but is instead oxomolybdenum tetramesitylporphyrin [(TMP)MoO] (1). The presence of an oxo on one side of the porphyrin plane explains why the literature ¹H NMR spectrum (which matches ours) shows the expected number of peaks for C_{4v} rather than D_{4h} symmetry. ⁵⁶ Supporting this assignment, the IR spectrum displays a Mo=O stretch at 1005 cm⁻¹, which is near the 952-980 cm⁻¹ range of Mo=O frequencies in other oxomolybdenum(IV) porphyrin complexes, but is unusually strong due to the absence of a trans ligand.⁵⁹ The electronic absorption spectrum of 1 is normal for a metalloporphyrin, with a Soret band at 431 nm ($\varepsilon = 207$ cm⁻¹ mM⁻¹), β band at 554 nm (11 cm⁻¹ mM⁻¹), and α band at 641 nm (4.2 cm⁻¹ mM⁻¹).

Addition of 100 equiv. of HCl etherate (2 M in Et₂O) to a toluene solution of (TMP)MoO resulted in the formation of dichloromolybdenum tetramesitylporphyrin [(TMP)MoCl₂] (2) after several hours. Removal of volatile materials and washing with pentane and toluene afforded pure 2 as a green powder in 57% yield. Crystals of 2 suitable for X-ray diffraction were grown from diffusion of pentane into a concentrated solution in CH₂Cl₂ at -35 °C (crystallized yield 47%). Complex 2 is paramagnetic and the peaks in the ¹H NMR spectrum are shifted significantly from that of the parent ligand and 1. The β-proton signals appear at 17.3 ppm and the mesityl *m*-H signals shift to 6.80 ppm. The chemical shifts of the mesityl CH₃ peaks are relatively unaffected by the metal, though the *o*-CH₃ protons give a single peak integrating to 24H, indicating a plane of symmetry containing the porphyrin. The solution magnetic moment using the Evans method⁶⁰ was μ_{eff} = 2.1 μ_B, which is somewhat lower than expected for the S = 1 ground state of an octahedral d² complex. It is possible that the low magnetic moment arises from zero-field splitting, but further description

of the magnetism is beyond the scope of this paper. The visible spectrum of **2** shows a band with $\lambda_{max} = 359$ nm ($\epsilon = 38$ cm⁻¹ mM⁻¹) and other bands at 378 nm (36 cm⁻¹ mM⁻¹), 456 nm (9.3 cm⁻¹ mM⁻¹), 513 nm (6.8 cm⁻¹ mM⁻¹) and 592 nm (4.0 cm⁻¹ mM⁻¹). All of the spectroscopic characteristics of **2** are similar to the previously reported (TTP)MoCl₂ and (OEP)MoCl₂.^{61,62}

The reassigned metalation product, (TMP)MoO, was converted into nitridomolybdenum tetramesitylporphyrin, (TMP)MoN (3), according to literature procedures using Me₃SiN₃. Despite the misassignment of 1 in the literature, the procedure was effective and proceeded as reported. Our UV-Vis, IR, and EPR spectra of 3 matched the literature report, as did an X-ray crystal structure.⁵⁶

Crystallographic Characterization of Molybdenum Porphyrin Complexes

Complex 1 crystallizes in the space group P1 with two (TMP)MoO molecules and partial occupancy of a toluene per unit cell. The molybdenum atom is shifted out of the plane of the pyrrole nitrogen atoms toward the oxo ligand by 0.64 Å. This is reflected in the average N-Mo-O angle of 107.4° and the average N-Mo-N angle between trans porphyrin N atoms of 145.2°. The ring has distorted from a planar geometry to form a dome shape, as demonstrated by all four pyrrole nitrogen atoms being above the mean plane of the macrocycle in the normal-coordinate structural decomposition (NSD) (see SI). The average Mo-N distance is 2.127 Å, slightly elongated from the 2.100 Å average of six-coordinate (Por)MoV(O) complexes. The Mo-O distance is 1.656 Å, consistent with the bond lengths of (TPP)MoO and other (Por)MoV oxo complexes from the CCSD, which average 1.68 Å.63 The X-ray crystal structure of 1 is shown in Figure 3, and further details are in the supporting information.

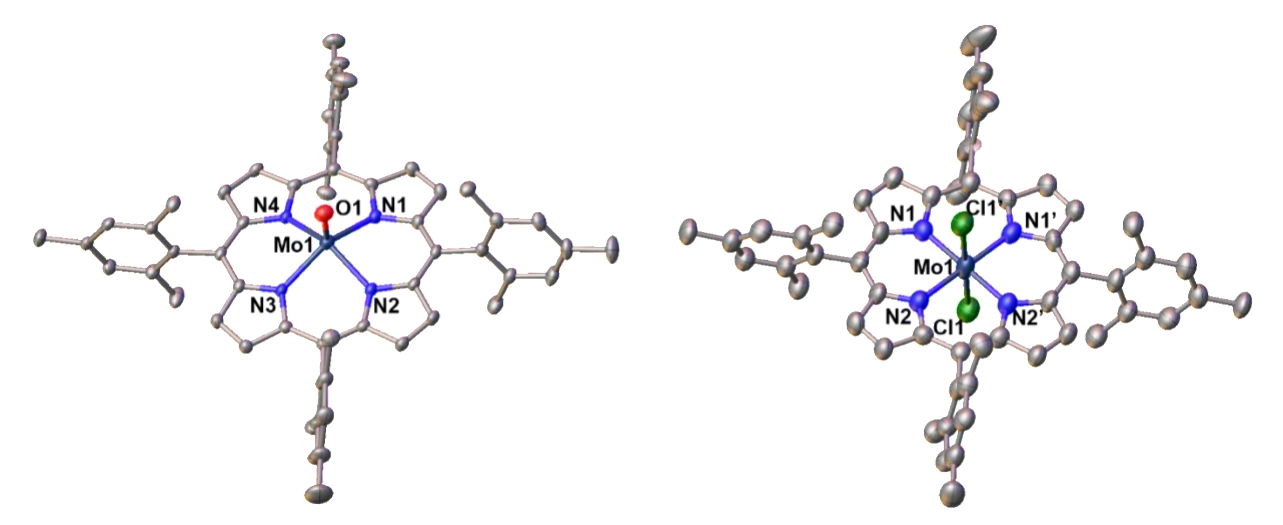


Figure 3: X-ray crystal structures for **1** (left) and **2** (right). Hydrogen atoms and disordered toluene molecules are omitted for clarity. Atoms with the (') mark in the structure of **2** are generated with the symmetry operator (1-X, +Y, 3/2-Z). Ellipsoids are shown at 50% probability.

Complex 2 crystallizes in the space group C2/c with four (TMP)MoCl₂ molecules and eight disordered toluene molecules per unit cell. The molybdenum lies on a 2-fold rotation axis that passes through opposite meso-carbon atoms, making the asymmetric unit half of the porphyrin ring with Mo-Cl and one disordered toluene. The crystal structure for one molecule of 2 is shown

in Figure 3. The Cl(1)-Mo-Cl(1') angle is $179.4(1)^{\circ}$. Unlike 1, the molybdenum lies very close to the plane of the four pyrrole nitrogen atoms, as shown by the angles at molybdenum; N(2)-Mo-N(1') = N(2')-Mo-N(1) = $179.7(3)^{\circ}$. The other angles surrounding molybdenum are roughly 90° . The Mo-N bond lengths are 2.055(6) and 2.057(6) Å and the Mo-Cl distance is 2.353(2) Å. These are similar to the distances in (TTP)MoCl₂.^{61,62}

Electrochemistry and Spectroelectrochemistry of Molybdenum Porphyrins

The redox properties of TMP and its molybdenum complexes were examined using cyclic voltammetry (CV) of solutions in THF using 0.2 M tetrabutylammonium hexafluorophosphate (TBAPF₆) electrolyte, under an N₂ atmosphere using a glassy carbon (GC) working electrode, a platinum wire counter electrode, and a silver wire pseudo reference electrode. Potentials were referenced to a ferrocene internal standard. Reduction potentials for TMP complexes are reported in Table 2 and shown in Figure 4. CV of the parent tetramesitylporphyrin (Figure 4A) showed the four redox events expected for oxidation and reduction of the porphyrin ring, two in each direction from the open-circuit potential (OCP) of -0.42 V vs Fc⁺/Fc. The oxidative features were quasireversible, and reversibility decreased with scan rate, suggesting the generation of an unstable species, whose nature is unknown. The two reductive events, which are of greater interest here, were electrochemically reversible and had mid-point potentials of -1.82 V and -2.29 V vs Fc⁺/Fc. UV-vis spectroelectrochemical measurements (UV-SEC) performed in an OTTLE (optically transparent thin-layer electrode) cell⁶⁴ showed that electrolysis at the first reduction potential caused a decrease of the Soret band and Q-peaks associated with TMP and the growth of new broad features at 454, 631, 692, and 776 nm (Figures S32-33). These spectral observations are consistent with reduction of TMPH2 to a radical anion. 65,66 During reduction at the second reduction potential, the Soret band decreased further in intensity, the new absorbances at 692 and 776 nm disappeared, the feature at 454 nm grew and shifted to 443 nm, and new peaks grew in at 564 and 612 nm. The spectra of the radical anion and TMPH2 were regenerated upon returning the potential of the electrode.

Table 2: Reduction potentials of TMP complexes as 1 mM solutions in 0.2 M [NBu₄]PF₆ in THF. All potentials are referenced to the Fc⁺/Fc couple.

	E _{1/2} (Mo-based)	E _{1/2} (TMP ^{/-})	E _{1/2} (TMP ^{0/-} -)	$E_{1/2} \ (TMP^{\cdot +/0}) \ or \ Mo^{V/IV}$	$E_{1/2}$ (TMP+/·+)
TMPH ₂		-2.29 V	-1.82 V	0.65 V	1.01 V
(TMP)MoO (1)	−3.26 V	-2.31 V	-1.69 V	−0.39 V	
(TMP)MoN (3)	−3.09 V	−2.27 V	-1.64 V		

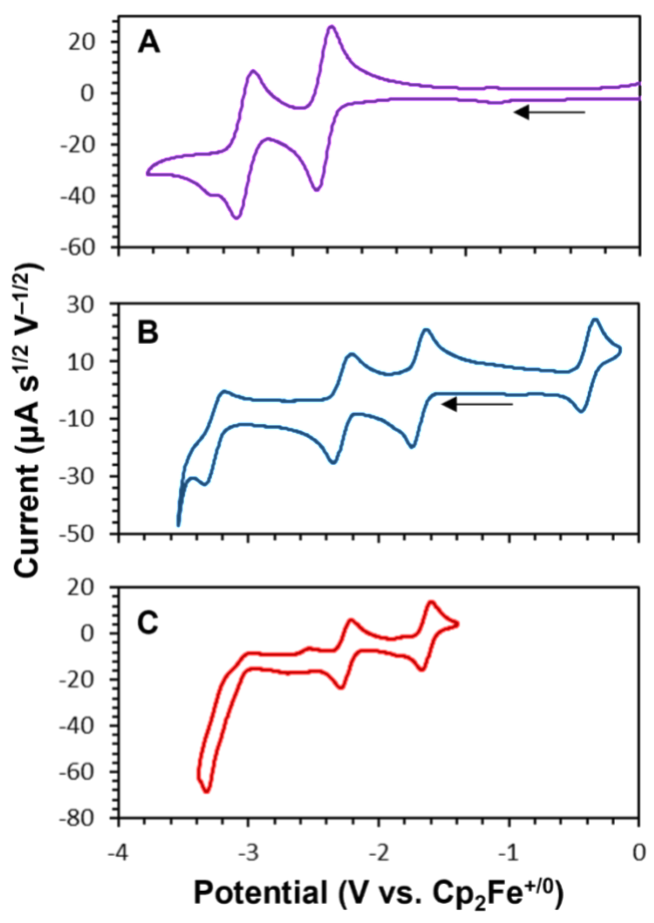


Figure 4: Cropped cyclic voltammograms of TMP complexes. A) CV of TMPH₂ at 25 mV/s. OCP = -0.42 V. B) CV of **1** at 250 mV/s. OCP = -1.1 V. C) CV of **3** at 25 mV/s. OCP = -0.29 V. See SI for full sweeps.

In the CV of oxo complex 1 (Figure 4B), four redox events were observed at -0.39 V, -1.69 V, -2.31 V, and -3.26 V vs Fc⁺/Fc. The redox wave at -0.39 V is more anodic than the OCP of -0.52 V, indicating that it is an oxidation. Previous studies on (TPP)Mo(O)(OMe) and (TPP)MoO have shown that the Mo^{V/IV} couple is the first reduction for the former and first oxidation for the latter, rather than a ligand based redox event.^{59,68-70} For (TTP)MoO, this feature appears at -0.46 V vs Fc⁺/Fc in CH₂Cl₂,^{70,71} supporting our analogous assignment of the redox couple at -0.39 V as [(TMP)MoO]^{+/0}. The first two reductions at -1.69 V and -2.31 V cause similar spectral changes to the visible absorbance of 1 by UV-SEC as observed for the first two reductions of TMPH₂ (Figure S37 & S38), and so we likewise assign them as TMP/TMP⁻ and TMP⁻/TMP²⁻. The first and second $E_{1/2}$ values associated with TMP in 1 are cathodically shifted from the ones in (TPP)MoO by 0.1 V and 0.4 V, respectively, as expected for a porphyrin with more electrondonating substituents. The most cathodic quasi-reversible feature at -3.26 V has not been described in reports on other (Por)MoO complexes and is tentatively assigned to Mo^{IV/III}.

We focused primarily on the nitride complex 3 because it could be an on-cycle species for nitrogen reduction. In the reductive CV of complex 3 (Figure 4C), there are redox events at -1.64 V, -2.27 V, and -3.09 V vs Fc⁺/Fc. UV-SEC measurements of an electrolysis at -1.7 V showed a decrease

of the porphyrin Soret band and Q-peaks as well as the appearance of new absorbances at 458, 622, 702, 722 and 778 nm, similar to the locations observed in the reduction of TMPH₂ to the radical anion (Figure 5A). Additional loss of visible absorbance was observed during reduction at -2.3 V, and as in the second reduction of TMPH₂ new peaks grew in at 450, 523, 568 and 618 nm (Figure 5B). Both UV-SEC processes were reversible, and electrolysis at -1 V resulted in the rapid regeneration of the original spectra. The similarity of all spectral changes to those observed in the reduction of 1 strongly suggests that the redox couples at -1.64 V and -2.27 V are ligand-based reductions, TMP/TMP⁻ and TMP⁻/TMP²⁻. These results follow the literature precedent set by (TMP)MnN and (OEP)ReN (OEP = octaethylporphyrin), in which all observed reductive electrochemical activity occurred at the ligand.^{66,67} Our tentative assignment for the most cathodic redox event (which is quasi-reversible) is Mo^{V/IV}; it is at a potential more negative than accessed in the literature reports.

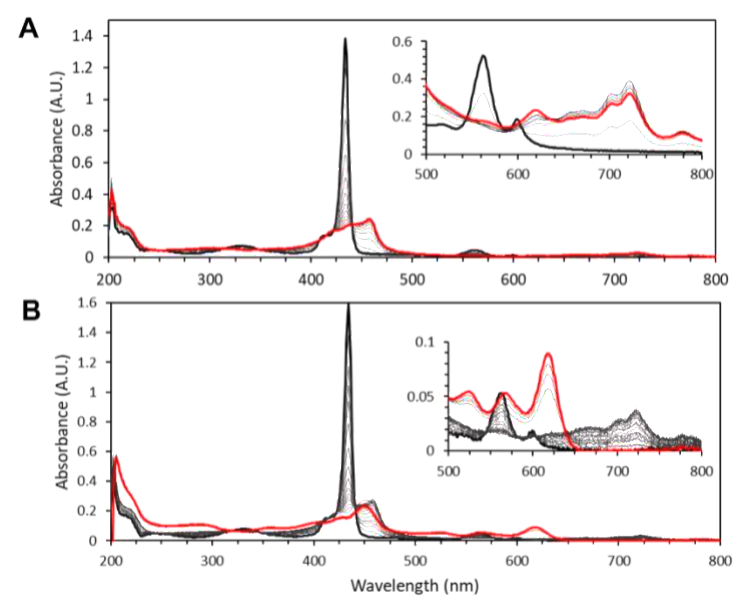


Figure 5: UV-SEC plots of the reductions of 0.2 mM nitride **3**, initial scans prior to electrolysis are shown in black, final scans after electrolysis are shown in red. A) Electrolysis at -1.7 V vs Fc⁺/Fc. B) Electrolysis **3** at -1.5 V vs Fc⁺/Fc, before stepping the potential to -2.3 V vs Fc⁺/Fc. Insets for A and B show the 500-800 nm range for a solution of 2.5 mM **3**.

Determining the N-H BDFE of the Imidomolybdenum(IV) Species

Previous work has shown that protonation of (TMP)MoN with hydrochloric acid⁵⁶ and Lewis acids⁷² occurs at the nitride, but the p K_a of (TMP)MoNH⁺ was not determined. Taking advantage of the sensitivity of the visible spectrum to changes at the Mo–N unit, we titrated pyridinium triflate ([PyH][OTf]) into a solution of (TMP)MoN in THF. The visible spectra showed conversion with isosbestic points to a new species (Figure S49), in a process that was reversible upon addition of triethylamine as a base. The changes in absorbance enabled us to calculate the equilibrium constant (K_{eq}) for the reaction. Using the tabulated p K_a of pyridine (5.5 in THF),⁷³ the p K_a of [(TMP)MoNH]⁺ in THF is calculated to be 3.8.

Conversion to the protonated nitride complex was accomplished by adding triflic acid (TfOH, p K_a = 0.7 in MeCN)^{74,75} or diphenylammonium triflate ([Ph₂NH₂][OTf], p K_a = 3.2 in THF, p K_a = 5.9 in MeCN),⁷⁶ as verified by comparison of the visible spectrum to that of the titration above, and by the appearance of an N-H stretching band at 3253 cm⁻¹ in the IR spectrum. Cyclic voltammetry of (TMP)MoNH⁺ generated in this way reveals two overlapping redox features that are anodically shifted from the first reduction potential of **3** (Figure 6, top). Both of these features correspond to one electron processes. The first irreversible feature at E_{pc} = -0.98 V vs Fc⁺/Fc causes a change in the visible spectrum by UV-SEC that corresponds to formation of the parent nitride **3** (Figure 6, Bottom). The lack of a return wave for the initial reduction indicates that the lifetime of the reduced (TMP)Mo^{IV}=NH is quite short under these conditions, and bubbles in the SEC cell following prolonged electrolysis at -1.0 V suggest that H₂ formation is responsible for the decomposition back to **3**. The second feature ($E_{1/2}$ = -1.15 vs Fc⁺/Fc) is reversible, and it causes changes in the visible spectrum that are consistent with protonation of the TMP ligand (see SI). However, our understanding of the cathodic chemistry of **3** is incomplete.

Assuming that the irreversible cathodic feature at -0.98 V is the reduction of (TMP)MoNH⁺, we can estimate that $E_{1/2} \sim -0.94$ V vs Fc⁺/Fc for the (TMP)MoNH⁺/(TMP)MoNH couple (see SI). The reduction potential of the nitride and p K_a of the imido complex can be used to calculate the metal imido BDFE, through the relation $BDFE = 23.06E^{\circ} + 1.37$ p $Ka + C_G$.^{13,77,78} Using this method, we estimate the imido N-H BDFE to be 43±2 kcal/mol.^{13,77} This is a rare example of an experimentally determined imido N-H BDFE, and it is similar to those calculated for other Mo=NH species which range from 37 to 64 kcal/mol.^{42,79-81}

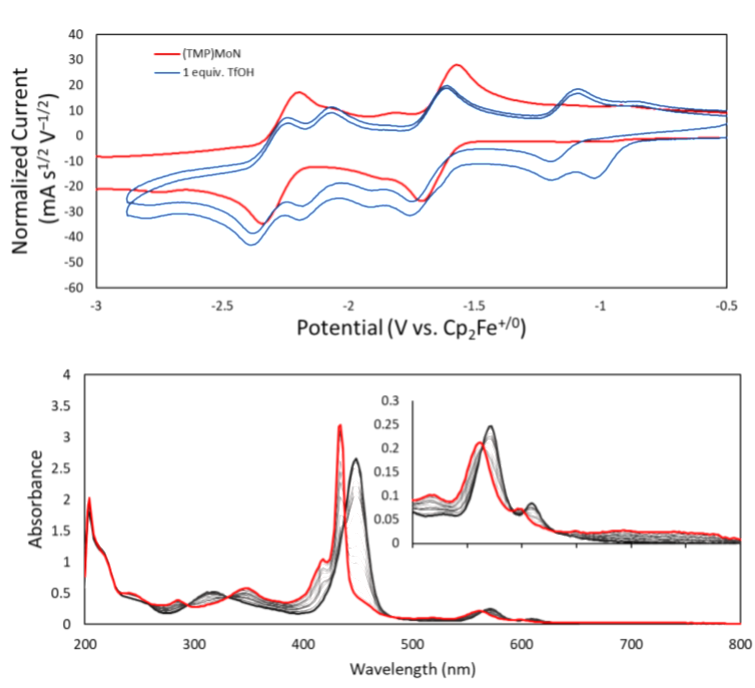


Figure 6: Top) Reductive CV of **3** (red) compared to that of **3** when protonated by 1 equivalent of triflic acid (blue). Bottom) UV-SEC of **3** in the presence of 1 equivalent of TfOH, stepping the potential from -0.7 V (black trace) to -1 V vs Fc⁺/Fc (red trace).

To support this estimate of the BDFE, we turned to DFT computations at the B3LYP/SARC-def2-TZVP level. The imido BDFE was calculated from the free energies (ΔG) of a hypothetical hydrogen atom transfer reaction with varying acceptors. The literature values for the BDFE of the acceptor-H bond were used as a reference (eq 1 and 2):

$$(TMP)Mo = NH + A$$
 $\xrightarrow{\Delta G^{\circ}} (TMP)Mo \equiv N + A - H$ Eq. 1
 $BDFE(NH) = \Delta G^{\circ}(NH) + BDFE_{(expt)}(A - H)$ Eq. 2

The free energy of the putative Mo^{IV} imido complex was computed for both the S=1 high-spin configuration, which has one electron in a Mo d_{xz} orbital and the other delocalized in the porphyrin ring, and for the S=0 low spin configuration, where the HOMO is a doubly occupied Mo d_{xy} orbital. The single point energy of the singlet was lower than the triplet by 4.8 kcal/mol, which lies within the uncertainty limits of DFT single point energy calculations. The similarity of energy indicates that the pairing energy in the singlet is similar to the energy gap between the lowest-energy molybdenum d-orbital and the porphyrin LUMO. This in turn shows the feasibility of redox activity of the porphyrin during catalysis, which agrees with the spectroelectrochemical results above.

A variety of H-atom acceptors were examined as references, and the results are shown in Table 3. The values for the high-spin configuration computed using metallocene H-atom acceptor/donor pairs are fairly close to the experimentally estimated value of 43 kcal/mol. We highlight an important caveat, that the values from DFT computations are highly variable, and depend on the H-atom acceptor used as a reference. This suggests that DFT has difficulty accurately assessing the BDFEs of these standard compounds! We have not been able to resolve these computational inaccuracies, and we report here the various outcomes rather than choosing one reference point as a "gold standard."

Table 3: Computed molybdenum imido N-H BDFEs with reference to experimental H-atom transfer reagents. The Co(II, NH)⁺ notation refers to Peters's PCET mediator.²⁸ BDFEs were computed for both high and low spin (TMP)Mo=NH configurations.

	Acceptor	Calculated Imido	Calculated Imido	
H-Atom Acceptor	Experimental BDFE	BDFE (low-spin)	BDFE (high-spin)	
	(kcal/mol)	(kcal/mol)	(kcal/mol)	
TEMPO/TEMPOH	65.5 ⁷⁸	53.1	48.3	
Co ^{III} Cp* ₂ /Co ^{II} Cp*(C ₅ Me ₅ H)	2982	49.1	44.3	
Co(III, N) ⁺ /Co(II, NH) ⁺	38.983	46.6	41.8	

Chemical Catalysis

Considering the weak N–H bond in the imidomolybdenum(V) complex, we chose reagents for chemical PCET with excellent ability to donate protons and electrons. The thermodynamic ability of a reductant/acid pair to donate an H• equivalent is termed the "effective BDE," and we chose SmI₂/ethylene glycol, a reagent with a particularly low effective BDE of 25 kcal/mol,⁸⁴ providing almost 20 kcal/mol of driving force for the first N-H bond formation. The results of these chemical catalysis experiments following the reaction in Equation 3 are tabulated in Table 4. Catalysis with nitride 3 and 180 equiv. of SmI₂/ethylene glycol led to the formation of 33 equivalents of ammonia

per molybdenum center, which corresponds to a 55% yield based on samarium. Another 30% of electrons can be attributed to formation of H₂, and the fate of the remaining 17% is unknown. The oxo complex 1 produced 25 equivalents of NH₃ at 42% yield, making 44 equivalents H₂ (49%) in the process. Using dichloride 2 as a precatalyst under these conditions resulted in only 15 equivalents of NH₃ per molybdenum at a more modest yield of 25%, explained by a greater production of H₂ (55%). It should be noted that in trials using a setup that was not amenable for headspace analysis, the amount of NH₃ produced and electron efficiency were higher for both dichloride 2 and nitride 3, generating 42-43 equivalents NH₃/Mo with a yield of 58-62%. Ammonia formation with 3 was also observed when using [HNEt₃][PF₆]/CoCp*₂, an acid and reductant combination with an effective BDFE of 35 kcal/mol, which gives it 10 kcal/mol less driving force than SmI₂/ROH. In this reaction, 2.8 equivalents of ammonia per molybdenum were produced, with an efficiency in CoCp*₂ use of only 5%.

$$N_2 + 6 \text{ SmI}_2(\text{THF})_2 + 6 (\text{CH}_2\text{OH})_2 \xrightarrow{\text{[Mo Catalyst]}} 2 \text{ NH}_3 + 6 \text{ SmI}_2(\text{OR}) (+ \text{H}_2) \text{ Eq.3}$$

Table 4: Results for chemical catalysis trials following the reaction shown in Equation 3 with molyhdenum tetramesitylnorphyrin complexes as the catalyst

Catalyst	Equiv.	Equiv.	% Yield	Equiv.	% Yield	Electron
Catalyst	SmI ₂ /ROH	NH ₄ ⁺ / Mo	NH ₃ ^a	H ₂ / M ₀	H ₂ ^a	Yielda
(TMP)MoOb	180	25.3 ± 0.5	$42.2 \pm 0.8\%$	44 ± 4	$49 \pm 4\%$	91±5%
(TMP)MoCl ₂ ^b	180	15 ± 3	25 ± 6%	51 ± 14	55 ± 15%	80±15%
(TMP)MoN ^b	180	33 ± 3	55% ± 4.5%	25 ± 11	$28 \pm 13\%$	83±13%
(TMP)MoCl ₂	200	42	58%			
(TMP)MoN ^b	200	43	62%			
(TMP)MoN ^c	13800	98	2%			
(TMP)MoN ^d	100	0.6	2%			
(TMP)MoN ^e	140	26	56%			

a) Defined as the yield based on SmI₂. b) Average of 3 trials. c) ROH = H_2O . d) Argon atmosphere. e) $^{15}N_2$ atmosphere.

To confirm that the ammonia observed was derived from N₂, the following control reactions were performed. A catalytic run under an argon atmosphere beginning from **3** produced 0.6 equiv. of ammonia per molybdenum center, which is less than the amount that would be expected for even stoichiometric conversion of the nitride ligand. This test shows that there is a negligible amount of ammonia from porphyrin degradation or work-up protocols. A further control was to perform the catalytic reaction under an atmosphere of ¹⁵N₂: this produced ¹⁵NH₄Cl with >98% ¹⁵N, as observed by ¹H NMR spectroscopy. This further confirms that the ammonia is generated from N₂.

The visible absorption spectrum of the solution following catalysis lacks characteristic porphyrin absorbances (Figure S48), which suggests reduction (and possible protonation) of the porphyrin ring. Despite the loss of the spectroscopic features associated with the porphyrin ring, when a completed reaction was supplied with more SmI₂/(CH₂OH)₂, we observed additional production of ammonia, indicating the presence of some catalytically active species in solution. This activity was unaffected by a drop of mercury, suggesting that the catalysis was not due to molybdenum

nanoparticles (Table S1). The identification of all of the catalytically active species is an ongoing challenge.

3. Discussion

N2 Reduction to NH3 at Molybdenum Catalysts

The three TMP molybdenum (pre)catalysts examined were all capable of producing NH₃ with SmI₂/ROH under 1 atm N₂ at room temperature. The nitrogen source was confirmed to be N₂ gas, using control reactions under argon and ¹⁵N₂. The molybdenum nitride catalyst achieved good turnover numbers for N₂ to NH₃ (33-43 equiv.) with moderate electron efficiencies based on samarium (55-62%). These results are similar to the 40-55 equiv./Mo reported for molybdenum phosphine pincer precatalysts under similar conditions.²¹ The molybdenum porphyrin catalysts are less efficient than literature pincer-molybdenum complexes, using only 25–62% of the provided reducing equivalents towards N₂ reduction. The lowered efficiency is explained by the production of H₂, 28-49%, respectively, compared to 4-22% for the previously reported examples.²¹ Ligand-mediated HER following porphyrin protonation has been previously observed in several systems.⁸⁵⁻⁸⁸ Based on these precedents, we propose that ligand protonation and reduction contributes to hydrogen production during catalysis.

Development in homogeneous NRR catalysis has mostly focused on pincer-type ligands. Nishibayashi published the second N₂-to-NH₃ catalytic system using a pyridine-based PNP pincer as the supporting ligand in a dinitrogen bridged complex, [(PNP)Mo(N₂)₂]₂(N₂),⁸⁹ and other catalysts bearing pincer ligands soon followed. Each of these systems achieve moderately successful catalysis with metallocene-based reducing agents and acid, ranging from approximately 5-15 equiv./M.¹⁸ Catalysis is much more successful using SmI₂/ROH as a PCET reagent, and systems with pincer ligands achieve up to 55 equivalents/M under conditions similar to our system. 18 With larger amounts of samarium, a (PCP)MoCl₃ catalyst achieved 4350 equiv./Mo (91%),²¹ the highest reported to date for a homogeneous catalyst. There are comparatively fewer examples of tetradentate ligands, and most of those reported are tripodal in contrast to the planar ligand described here, such as Schrock's seminal N2-to-NH3 catalyst (HIPTN3N)Mo(N2) (Figure 7).31 These systems generate 10-100 equiv. of NH₃/M with Cp₂M/acid reagents, and some perform electrocatalysis with Peters's mediator. 28,31,76 To our knowledge they have not been tested for catalysis with SmI₂/ROH, so direct comparison to our system is difficult. Metals coordinated to four ligands in one plane are represented by the Chatt-type M⁰ catalysts, which give yields in the range of 1-38 equiv./Mo (8-64%) with HOCH2CH2OH as the proton source, and up to 40 equiv./Mo (68%) using water instead. 18,30,90 Deviating from the simple mono- and bidentate phosphines originally published, recent work on linking the donor atoms has led to pentadentate complexes with an axial ligand trans to the N₂ binding cite.⁹¹ One such catalyst generated 26 equiv. of NH₃/Mo (43%) with SmI₂/ROH.⁹⁰ Few ligands studied in NRR contain only N-donor atoms, and to the best of our knowledge, only (HIPTN₃N)MoN₂ and the NNN-pincer shown in Figure 7 are catalytically active. 31,92 Other systems used pyridine diimine (PDI), terpyridine, and pentapyridyl as ligands for ammonia oxidation with molybdenum complexes. ^{79,80,93} Our porphyrin complex provides an example of NRR catalysis with all N-atom donors and a rigid planar geometry.

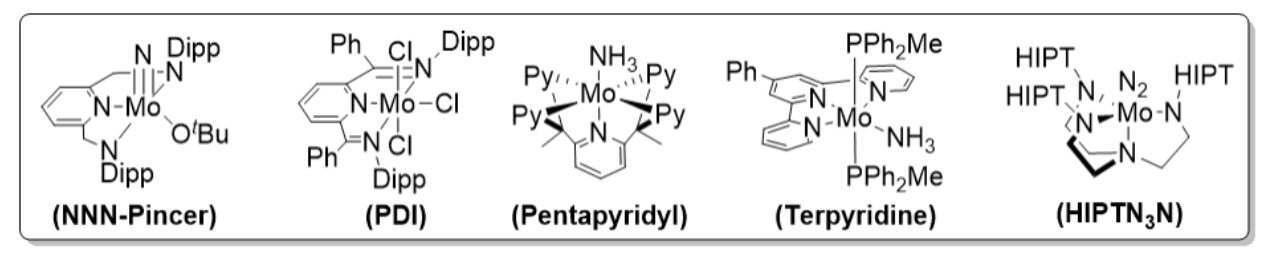


Figure 7: NRR related molybdenum complexes with all N-donor atoms. Dipp = diisopropylphenyl. HIPT = $3.5-(2.4.6-iPr_3C_6H_2)_2C_6H_3$.

NRR with Metalloporphyrins and Mechanistic Insights

Porphyrins have only recently appeared in the study of nitrogen cycle reactions, primarily focusing on metalloporphyrins immobilized onto solid supports acting as "single atom catalysts" in eNRR.52,53 TPP metalloporphyrins have been reported to produce ammonia from N2 in aqueous HCl while loaded on a carbon paper electrode. 52 (TPP)Co, (TPP)Cu, and (TPP)Mn formed NH₃ at a rate of 0.59, 0.42, and 0.31 equivalents metal⁻¹ h⁻¹, respectively (assuming an electrode area of 1 cm² and catalyst loading of 1 mg/cm²). The Faradaic efficiencies of the systems were 11%, 6%, and 4%. Following 2 h of electrocatalysis, electron microscope images of the electrode showed little change to the (TPP)Co catalyst. Another example evaluated 2D MOFs of tetrakis(4carboxyphenyl)porphyrin (TCPP) which were bound together by zinc ions and loaded onto a carbon paper support.⁵³ (TCPP)Fe achieved 2.9 equiv. of NH₃ Fe⁻¹ h⁻¹, at a Faradaic efficiency of 16.2%. The cobalt and zinc analogs generated 1.84 and 1.28 equiv. of NH₃ metal⁻¹ h⁻¹ at efficiencies of 11.6% and 6.4%. Turning to homogeneous chemistry, another report describes a well-defined (TMP)Ru(NH₃)₂ catalyst for ammonia oxidation to dinitrogen using H-atom abstraction reagents.⁵¹ Their work provides a possible microscopic reverse for the reaction performed by our TMP catalysts, and they propose N-N coupling from two ruthenium amido complexes to form a hydrazine bridged dimer. Computations support this pathway in their system energetically and these results match well with previous experimental work on stoichiometric NH₃ oxidation by a ruthenium diporphyrin system. 94,95 This body of work, while performing the reverse reaction from our NRR catalysis shows that it is reasonable to form a N₂ bridged porphyrin dimer, even with a bulky ligand like TMP. Further, computational studies of diporphyrin systems for NRR support a mechanism of protonating and reducing a bound N₂ molecule rather than splitting to two terminal metal nitrides, ⁹⁶ but there is currently no experimental evidence for either pathway.

One aspect that was not investigated in the earlier reports is the possibility of metal-ligand cooperativity. In the system described here, our spectroelectrochemical investigations indicate that the porphyrin ligand is reduced by two electrons without any formal change to the oxidation state of the metal. It is possible that protonation of the ligand occurs following reduction (Figures S34-S35), and that a similar reduction and protonation occurs with PCET reagents during catalysis. Ligand protonation is precedented in N₂ chemistry. For example, the family of complexes LReCl₂ (L = [N(CH₂CH₂P'Bu₂)₂]⁻ or N(CHCHP'Bu₂)₂)^{97,98} is capable of splitting N₂ upon reduction, but the nitrides that result (LReNCl) both protonate at the ligand rather than on the nitride. In one case, protons on the ligand productively transferred to a nitride ligand. Addition of 1 equivalent acid to the PNP ruthenium complex [(HN(CH₂CH₂P'Bu₂)₂)RuN]⁺ resulted in the formation of an ammonia complex, with two protons moving from the ligand to the imido ligand generated from

protonation by the exogenous acid. 99 As noted above, some porphyrin systems have been shown to exhibit ligand-based reactivity upon reduction in the presence of protons, and others productively transfer H⁺ to axial heteroatom ligands, such as in O₂ reduction. 46 We suspect that the ability to reduce the ligand contributes to acid degradation of the complex in our system, as shown by the disappearance of the characteristic porphyrin bands upon reduction/protonation. However, reduction of the porphyrin may also serve to enhance reactivity of the typically stable metal nitride species by storing multiple electron equivalents before protonation at the nitride. While we have shown that protonation and reduction of the macrocycle does not prevent further catalysis, it is not clear whether the active species are porphyrins or reduced/protonated porphyrin derivatives. The mechanism of NRR in this system is the subject of ongoing work, and will guide new ligand designs.

Molybdenum Imido N-H BDFEs in NRR

The imido BDFE gives insight into which reagents will achieve productive NRR reactivity, but there are few BDFE values known in the literature for NRR catalysts. Values reported are predominantly computed values rather than experimentally determined BDFEs, though some of the computational results are supported by BDFE bracketing or calorimetric measurements. Among the molybdenum imido BDFEs the values range from 37–64 kcal/mol,^{42,79-81} though [(PY5)MoNH]²⁺ is a notable outlier with its BDFE of 64 kcal/mol.⁷⁹ The rest of those reported span from 37–56 kcal/mol. For (TPP)Mo(NH₃)(N-H), a close analogue of **3**, the BDFE_{calc} was 56 kcal/mol,⁴⁰ though this is likely affected by the ligand trans to the nitride. Our experimentally estimated imido BDFE of 43 kcal/mol is similar to these computed values, though this may be inaccurate because the electrochemical reduction of the protonated nitride was irreversible, forcing us to estimate *E*_{1/2}.

The theoretical BDFEs computed with equations 1 and 2 agree reasonably well with the BDFE_{expt}. The computed values range 6.5 kcal/mol in energy (ignoring the 4.8 kcal/mol difference between the LS and HS configurations), and for the high-spin configuration deviates from the experimentally derived value by less than 5 kcal/mol. This is similar to the 4.7 kcal/mol difference reported for the (HIPTN₃N)MoN=N-H BDFE, and not as close as the 0.7 kcal/mol difference observed for [(Ph Tpy)(PPh₂Me)₂Mo(NH₂-H)]⁺.80 To the best of our knowledge, there are no other experimentally determined imido NH BDFEs in the literature for comparison. In addition, some of the variability in calculated values could be due to our implicit representation of solvation in the DFT model rather than explicit solvent coordination, which a computational study on (HIPTN₃N)Mo(N₂) found was more accurate in determining energies for protonation steps. ¹⁰⁰ Despite the variability of the calculations, the ΔG_{comp} for the reaction in Equation 1 correctly predicts the favorability of a HAT reaction with each H-atom acceptor based on the BDFE_{expt} of 43±2 kcal/mol.

4. Conclusions

Molybdenum complexes supported by the bulky tetramesitylporphyrin (TMP) are capable of catalytic reduction of N₂ to ammonia using SmI₂/ROH as a PCET reductant. Electrochemical and spectroelectrochemical studies have enabled us to estimate the BDFE of (TMP)MoNH as 43 kcal/mol, which quantifies the thermodynamics of the important first PCET step to the

molybdenum(V) nitride. The porphyrin supporting ligand is quite different than the phosphine-based supporting ligands that dominate in the literature, but performs similarly with up to 100 equiv. of ammonia formed per Mo, and efficiencies up to 60%. Catalyst decomposition and H₂ formation are challenges in this chemistry, and future work will take advantage of the tunable porphyrin scaffold for systematic improvement.

Author Contributions

A.S.H. performed all experiments, interpreted data, and wrote the manuscript. B.Q.M. advised on the crystallography. A.J.M.M. and P.L.H. provided supervision and edited the paper.

Conflicts of Interest

There are no conflicts to declare.

Acknowledgments

This work was supported by the U.S. National Science Foundation (CHE-1954254). The authors thank Dr. Jose Alvarez-Hernandez for assistance with gas chromatography, Reagan Hooper for fitting of the EPR data, and Dr. Jeremy E. Weber and Noah McMillion for helpful discussions.

References

- 1 S. J. K. Forrest, B. Schluschaß, E. Y. Yuzik-Klimova and S. Schneider, *Chemical reviews*, 2021, **121**, 6522-6587 (DOI:10.1021/acs.chemrev.0c00958).
- 2 V. Smil, *Nature*, 1999, **400**, 415 (DOI:10.1038/22672).
- 3 D. Mallamace, G. Papanikolaou, S. Perathoner, G. Centi and P. Lanzafame, *International Journal of Molecular Sciences*, 2021, **22** (DOI:10.3390/ijms22010139).
- 4 G. Hochman, A. S. Goldman, F. A. Felder, J. M. Mayer, A. J. M. Miller, P. L. Holland, L. A. Goldman, P. Manocha, Z. Song and S. Aleti, *ACS Sustainable Chem. Eng.*, 2020, **8**, 8938-8948 (DOI:10.1021/acssuschemeng.0c01206).
- 5 M. Jewess and R. H. Crabtree, *ACS Sustainable Chem. Eng.*, 2016, **4**, 5855-5858 (DOI:10.1021/acssuschemeng.6b01473).
- 6 The Oxford Institute for Energy Studies, https://www.oxfordenergy.org/publications/ammonia-as-a-storage-solution-for-future-decarbonized-energy-systems/, (accessed February 21, 2022).
- 7 K. Kugler, B. Ohs, M. Scholz and M. Wessling, *Phys. Chem. Chem. Phys.*, 2014, **16**, 6129-6138 (DOI:10.1039/C4CP00173G).

- 8 https://wcroc.cfans.umn.edu/research/renewable-energy/ammonia-synthesis, (accessed March 2, 2022).
- 9 https://www.aist.go.jp/fukushima/en/unit/HyCaT e.html, (accessed March 2, 2022).
- 10 O. Elishav, B. Mosevitzky Lis, E. M. Miller, D. J. Arent, A. Valera-Medina, A. Grinberg Dana, G. E. Shter and G. S. Grader, *Chem. Rev.*, 2020, **120**, 5352-5436 (DOI:10.1021/acs.chemrev.9b00538).
- 11 L. C. Caballero, N. E. Thornburg and M. M. Nigra, *Chem. Sci.*, 2022, (DOI:10.1039/D2SC04672E).
- 12 N. Lazouski, A. Limaye, A. Bose, M. L. Gala, K. Manthiram and D. S. Mallapragada, *ACS Energy Lett.*, 2022, **7**, 2627-2633 (DOI:10.1021/acsenergylett.2c01197).
- 13 M. J. Chalkley, M. W. Drover and J. C. Peters, *Chem. Rev.*, 2020, **120**, 5582-5636 (DOI:10.1021/acs.chemrev.9b00638).
- 14 Q. J. Bruch, G. P. Connor, N. D. Mcmillion, A. S. Goldman, F. Hasanayn, P. L. Holland and A. J. M. Miller, *Considering Electrocatalytic Ammonia Synthesis via Bimetallic Dinitrogen Cleavage*, American Chemical Society (ACS), 2020.
- 15 J. CHATT, A. J. PEARMAN and R. L. RICHARDS, *Nature*, 1975, **253**, 39-40 (DOI:10.1038/253039b0).
- 16 J. Chatt, A. J. Pearman and R. L. Richards, *J. Chem. Soc.*, *Dalton Trans.*, 1977, , 1852-1860 (DOI:10.1039/DT9770001852).
- 17 D. V. Yandulov and R. R. Schrock, *Science*, 2003, **301**, 76-78 (DOI:10.1126/science.1085326).
- 18 Y. Ashida and Y. Nishibayashi, *Chem. Commun.*, 2021, **57**, 1176-1189 (DOI:10.1039/D0CC07146C).
- 19 E. Laplaza Catalina and C. Cummins Christopher, *Science*, 1995, **268**, 861-863 (DOI:10.1126/science.268.5212.861).
- 20 J. J. Curley, T. R. Cook, S. Y. Reece, P. Müller and C. C. Cummins, *J. Am. Chem. Soc.*, 2008, **130**, 9394-9405 (DOI:10.1021/ja8002638).
- 21 Y. Ashida, K. Arashiba, K. Nakajima and Y. Nishibayashi, *Nature*, 2019, **568**, 536-540 (DOI:10.1038/s41586-019-1134-2).
- 22 I. Klopsch, M. Finger, C. Würtele, B. Milde, D. B. Werz and S. Schneider, *J. Am. Chem. Soc.*, 2014, **136**, 6881-6883 (DOI:10.1021/ja502759d).

- 23 A. Katayama, T. Ohta, Y. Wasada-Tsutsui, T. Inomata, T. Ozawa, T. Ogura and H. Masuda, *Angew. Chem. Int. Ed.*, 2019, **58**, 11279-11284 (DOI: https://doi.org/10.1002/anie.201905299).
- 24 J. E. Weber, F. Hasanayn, M. Fataftah, B. Q. Mercado, R. H. Crabtree and P. L. Holland, *Inorg. Chem.*, 2021, **60**, 6115-6124 (DOI:10.1021/acs.inorgchem.0c03778).
- 25 J. S. ANDERSON, J. RITTLE and J. C. PETERS, *Nature (London)*, 2013, **501**, 84-87 (DOI:10.1038/nature12435).
- 26 Q. J. Bruch, G. P. Connor, C. Chen, P. L. Holland, J. M. Mayer, F. Hasanayn and A. J. M. Miller, *J. Am. Chem. Soc.*, 2019, **141**, 20198-20208 (DOI:10.1021/jacs.9b10031).
- 27 S. Kuriyama, K. Arashiba, K. Nakajima, H. Tanaka, N. Kamaru, K. Yoshizawa and Y. Nishibayashi, *J. Am. Chem. Soc.*, 2014, **136**, 9719-9731 (DOI:10.1021/ja5044243).
- 28 P. Garrido-Barros, J. Derosa, M. J. Chalkley and J. C. Peters, *Nature*, 2022, **609**, 71-76 (DOI:10.1038/s41586-022-05011-6).
- 29 A. Eizawa, K. Arashiba, H. Tanaka, S. Kuriyama, Y. Matsuo, K. Nakajima, K. Yoshizawa and Y. Nishibayashi, *Nature Commun.*, 2017, **8**, 14874 (DOI:10.1038/ncomms14874).
- 30 Y. Ashida, K. Arashiba, H. Tanaka, A. Egi, K. Nakajima, K. Yoshizawa and Y. Nishibayashi, *Inorg. Chem.*, 2019, **58**, 8927-8932 (DOI:10.1021/acs.inorgchem.9b01340).
- 31 V. Ritleng, D. V. Yandulov, W. W. Weare, R. R. Schrock, A. S. Hock and W. M. Davis, *J. Am. Chem. Soc.*, 2004, **126**, 6150-6163 (DOI:10.1021/ja0306415).
- 32 K. Arashiba, H. Tanaka, K. Yoshizawa and Y. Nishibayashi, *Chem. Eur. J.*, 2020, **26**, 13383-13389 (DOI:10.1002/chem.202002200).
- 33 K. Arashiba, A. Eizawa, H. Tanaka, K. Nakajima, K. Yoshizawa and Y. Nishibayashi, *Bull. Chem. Soc. Jpn*, 2017, **90**, 1111-1118 (DOI:10.1246/bcsj.20170197).
- 34 J. Fajardo and J. C. Peters, *J. Am. Chem. Soc.*, 2017, **139**, 16105-16108 (DOI:10.1021/jacs.7b10204).
- 35 J. Fajardo and J. C. Peters, *Inorg. Chem.*, 2021, **60**, 1220-1227 (DOI:10.1021/acs.inorgchem.0c03354).
- 36 G. P. Connor, D. Delony, J. E. Weber, B. Q. Mercado, J. B. Curley, S. Schneider, J. M. Mayer and P. L. Holland, *Chem. Sci.*, 2022, (DOI:10.1039/D1SC04503B).
- 37 D. Wang, F. Loose, P. J. Chirik and R. R. Knowles, *J. Am. Chem. Soc.*, 2019, **141**, 4795-4799 (DOI:10.1021/jacs.8b12957).

- 38 B. D. Matson and J. C. Peters, *ACS Catal.*, 2018, **8**, 1448-1455 (DOI:10.1021/acscatal.7b03068).
- 39 M. J. Bezdek, I. Pappas and P. J. Chirik, in *Nitrogen Fixation*, ed. Y. Nishibayashi, Springer International Publishing, Cham, 2017, p. 1-21.
- 40 M. Barona, S. I. Johnson, M. Mbea, R. M. Bullock and S. Raugei, *Topics in Catalysis*, 2022, **65**, 341-353 (DOI:10.1007/s11244-021-01511-3).
- 41 A. Eizawa, K. Arashiba, A. Egi, H. Tanaka, K. Nakajima, K. Yoshizawa and Y. Nishibayashi, *Chem. Asian J.*, 2019, **14**, 2091-2096 (DOI:https://doi.org/10.1002/asia.201900496).
- 42 G. Stephan, C. Sivasankar, F. Studt and F. Tuczek, *Chem. Eur. J.*, 2008, **14**, 644-652 (DOI:10.1002/chem.200700849).
- 43 R. Zhang and J. J. Warren, *ChemSusChem*, 2021, **14**, 293-302 (DOI:10.1002/cssc.202001914).
- 44 X. Li, H. Lei, L. Xie, N. Wang, W. Zhang and R. Cao, *Acc. Chem. Res.*, 2022, **55**, 878-892 (DOI:10.1021/acs.accounts.1c00753).
- 45 K. Mittra, A. Singha and A. Dey, *Dalton Trans.*, 2016, **45**, 18796-18802 (DOI:10.1039/C6DT03597C).
- 46 J. Rosenthal and D. G. Nocera, *Acc. Chem. Res.*, 2007, **40**, 543-553 (DOI:10.1021/ar7000638).
- 47 L. Zou, R. Sa, H. Lv, H. Zhong and R. Wang, *ChemSusChem*, 2020, **13**, 6124-6140 (DOI:10.1002/cssc.202001796).
- 48 E. M. Nichols, J. S. Derrick, S. K. Nistanaki, P. T. Smith and C. J. Chang, *Chem. Sci.*, 2018, **9**, 2952-2960 (DOI:10.1039/C7SC04682K).
- 49 E. A. Mohamed, Z. N. Zahran and Y. Naruta, *Chem. Commun.*, 2015, **51**, 16900-16903 (DOI:10.1039/C5CC04273A).
- 50 C. Huang, S. Lv, C. Li, B. Peng, G. Li and L. Yang, *Nano Research*, 2022, **15**, 4039-4047 (DOI:10.1007/s12274-021-4009-4).
- 51 P. L. Dunn, S. I. Johnson, W. Kaminsky and R. M. Bullock, *J. Am. Chem. Soc.*, 2020, **142**, 3361-3365 (DOI:10.1021/jacs.9b13706).
- 52 S. Sun, X. Yang, S. Li, X. Chen, K. Li, J. Lv, W. Wang, D. Cheng, Y. Wang and H. Zang, *Catal. Sci. Technol.*, 2021, **11**, 2589-2596 (DOI:10.1039/D1CY00022E).

- 53 M. Cong, X. Chen, K. Xia, X. Ding, L. Zhang, Y. Jin, Y. Gao and L. Zhang, *J. Mater. Chem. A*, 2021, **9**, 4673-4678 (DOI:10.1039/D0TA08741F).
- 54 S. Shang, W. Xiong, C. Yang, B. Johannessen, R. Liu, H. Hsu, Q. Gu, M. K. H. Leung and J. Shang, *ACS Nano*, 2021, **15**, 9670-9678 (DOI:10.1021/acsnano.0c10947).
- 55 J. T. Groves and T. Takahashi, *J. Am. Chem. Soc.*, 1983, **105**, 2073-2074 (DOI:10.1021/ja00345a071).
- 56 J. C. Kim, W. S. Rees and V. L. Goedken, *Inorg. Chem.*, 1994, **33**, 3191-3194 (DOI:10.1021/ic00092a030).
- 57 C. Yang, S. J. Dzugan and V. L. Goedken, *J. Chem. Soc.*, *Chem. Commun.*, 1986, , 1313-1315 (DOI:10.1039/C39860001313).
- 58 J. P. Collman, C. E. Barnes and L. K. Woo, *Proc. Natl. Acad. Sci. USA*, 1983, **80**, 7684-7688 (DOI:10.1073/pnas.80.24.7684).
- 59 Y. Matsuda and Y. Murakami, *Coord. Chem. Rev.*, 1988, **92**, 157-192 (DOI:10.1016/0010-8545(88)85008-2).
- 60 D. F. Evans, J. Chem. Soc., 1959, 2003-2005 (DOI:10.1039/JR9590002003).
- 61 T. Diebold, B. Chevrier and R. Weiss, *Angew. Chem. Int. Ed Engl.*, 1977, **16**, 788-789 (DOI:10.1002/anie.197707881).
- 62 T. Diebold, B. Chevrier and R. Weiss, *Inorg. Chem.*, 1979, **18**, 1193-1200 (DOI:10.1021/ic50195a004).
- 63 Groom, C.R., Bruno, I.J., Lightfoot, M.P. and Ward, S.C., *Acta Cryst. B*, 2016, **72**, 171-179 (DOI:10.1107/S2052520616003954).
- 64 M. Krejčik, M. Daněk and F. Hartl, *Journal of Electroanalytical Chemistry and Interfacial Electrochemistry*, 1991, **317**, 179-187 (DOI:10.1016/0022-0728(91)85012-E).
- 65 B. Dozza, B. M. Rodrigues, I. Tisoco, V. B. de Souza, L. Angnes and B. A. Iglesias, *Microchemical Journal*, 2022, **183**, 108041 (DOI:10.1016/j.microc.2022.108041).
- 66 C. Tong, J. A. Jones and L. A. Bottomley, *Inorg. Chim. Acta*, 1996, **251**, 105-109 (DOI:https://doi.org/10.1016/S0020-1693(96)05261-9).
- 67 L. A. Bottomley, F. L. Neely and J. N. Gorce, *Inorg. Chem.*, 1988, **27**, 1300-1303 (DOI:10.1021/ic00280a046).
- 68 Y. Matsuda, S. Yamada and Y. Murakami, *Inorg. Chem.*, 1981, **20**, 2239-2246 (DOI:10.1021/ic50221a060).

- 69 K. M. Kadish, T. Malinski and H. Ledon, *Inorg. Chem.*, 1982, **21**, 2982-2987 (DOI:10.1021/ic00138a014).
- 70 T. Malinski, P. M. Hanley and K. M. Kadish, *Inorg. Chem.*, 1986, **25**, 3229-3235 (DOI:10.1021/ic00238a028).
- 71 N. G. Connelly and W. E. Geiger, *Chem. Rev.*, 1996, **96**, 877-910 (DOI:10.1021/cr940053x).
- 72 Ju Chang Kim, Byung Min Lee, and I. S. Jong, *Polyhedron*, 1995, **14**, 2145-2149 (DOI:https://doi.org/10.1016/0277-5387(95)00009-H).
- 73 T. Rodima, I. Kaljurand, A. Pihl, V. Mäemets, I. Leito and I. A. Koppel, *J. Org. Chem.*, 2002, **67**, 1873-1881 (DOI:10.1021/jo016185p).
- 74 A. Kütt, T. Rodima, J. Saame, E. Raamat, V. Mäemets, I. Kaljurand, I. A. Koppel, R. Y. Garlyauskayte, Y. L. Yagupolskii, L. M. Yagupolskii, E. Bernhardt, H. Willner and I. Leito, *J. Org. Chem.*, 2011, **76**, 391-395 (DOI:10.1021/jo101409p).
- 75 A. J. Heyer, P. J. Shivokevich, S. L. Hooe, K. D. Welch, W. D. Harman and C. W. Machan, *Dalton Trans.*, 2018, **47**, 6323-6332 (DOI:10.1039/C8DT00598B).
- 76 M. J. Chalkley, T. J. Del Castillo, B. D. Matson, J. P. Roddy and J. C. Peters, *ACS Cent. Sci.*, 2017, **3**, 217-223 (DOI:10.1021/acscentsci.7b00014).
- 77 R. G. Agarwal, C. F. Wise, J. J. Warren and J. M. Mayer, *Chem. Rev.*, 2022, **122**, 1482 (DOI:10.1021/acs.chemrev.1c00791).
- 78 C. F. Wise, R. G. Agarwal and J. M. Mayer, *J. Am. Chem. Soc.*, 2020, **142**, 10681-10691 (DOI:10.1021/jacs.0c01032).
- 79 S. I. Johnson, S. P. Heins, C. M. Klug, E. S. Wiedner, R. M. Bullock and S. Raugei, *Chem. Commun.*, 2019, **55**, 5083-5086 (DOI:10.1039/C9CC01249D).
- 80 M. J. Bezdek, S. Guo and P. J. Chirik, *Science*, 2016, **354**, 730-733 (DOI:10.1126/science.aag0246).
- 81 C. C. Almquist, N. Removski, T. Rajeshkumar, B. S. Gelfand, L. Maron and W. E. Piers, *Angew. Chem. Int. Ed.*, 2022, **61**, e202203576 (DOI:10.1002/anie.202203576).
- 82 M. J. Chalkley, P. H. Oyala and J. C. Peters, *J. Am. Chem. Soc.*, 2019, **141**, 4721-4729 (DOI:10.1021/jacs.9b00193).
- 83 M. J. Chalkley, P. Garrido-Barros and J. C. Peters, *Science*, 2020, **369**, 850-854 (DOI:10.1126/science.abc1607).

- 84 S. S. Kolmar and J. M. Mayer, *J. Am. Chem. Soc.*, 2017, **139**, 10687-10692 (DOI:10.1021/jacs.7b03667).
- 85 R. Sun, M. Liu, S. Zheng, D. K. Dogutan, C. Costentin and D. G. Nocera, *Proc. Natl. Acad. Sci.*, 2022, **119**, e2122063119 (DOI:10.1073/pnas.2122063119).
- 86 B. H. Solis, A. G. Maher, D. K. Dogutan, D. G. Nocera and S. Hammes-Schiffer, *Proc. Natl. Acad. Sci.*, 2016, **113**, 485-492 (DOI:10.1073/pnas.1521834112).
- 87 A. G. Maher, M. Liu and D. G. Nocera, *Inorg. Chem.*, 2019, **58**, 7958-7968 (DOI:10.1021/acs.inorgchem.9b00717).
- 88 D. K. Bediako, B. H. Solis, D. K. Dogutan, M. M. Roubelakis, A. G. Maher, C. H. Lee, M. B. Chambers, S. Hammes-Schiffer and D. G. Nocera, *Proc. Natl. Acad. Sci.*, 2014, **111**, 15001-15006 (DOI:10.1073/pnas.1414908111).
- 89 K. Arashiba, Y. Miyake and Y. Nishibayashi, *Nature Chem.*, 2011, **3**, 120-125 (DOI:10.1038/nchem.906).
- 90 T. A. Engesser, A. Kindjajev, J. Junge, J. Krahmer and F. Tuczek, *Chem. Eur. J.*, 2020, **26**, 14807-14812 (DOI:10.1002/chem.202003549).
- 91 N. Stucke, T. Weyrich, M. Pfeil, K. Grund, A. Kindjajev and F. Tuczek, in *Nitrogen Fixation*, ed. Y. Nishibayashi, Springer International Publishing, Cham, 2017, p. 113-152.
- 92 L. A. Wickramasinghe, T. Ogawa, R. R. Schrock and P. Müller, *J. Am. Chem. Soc.*, 2017, **139**, 9132-9135 (DOI:10.1021/jacs.7b04800).
- 93 G. W. Margulieux, Z. R. Turner and P. J. Chirik, *Angew. Chem. Int. Ed.*, 2014, **53**, 14211-14215 (DOI:10.1002/anie.201408725).
- 94 J. P. Collman, J. E. Hutchison, M. A. Lopez and R. Guilard, *J. Am. Chem. Soc.*, 1992, **114**, 8066-8073 (DOI:10.1021/ja00047a015).
- 95 J. P. Collman, J. E. Hutchison, M. S. Ennis, M. A. Lopez and R. Guilard, *J. Am. Chem. Soc.*, 1992, **114**, 8074-8080 (DOI:10.1021/ja00047a016).
- 96 H. Wan, A. Bagger and J. Rossmeisl, *ChemRxiv.*, 2022, (DOI:https://doi.org/10.26434/chemrxiv-2022-79581).
- 97 R. S. van Alten, F. Wätjen, S. Demeshko, A. J. M. Miller, C. Würtele, I. Siewert and S. Schneider, *Eur. J. Inorg. Chem.*, 2020, **2020**, 1402-1410 (DOI:10.1002/ejic.201901278).
- 98 I. Klopsch, M. Finger, C. Würtele, B. Milde, D. B. Werz and S. Schneider, *J. Am. Chem. Soc.*, 2014, **136**, 6881-6883 (DOI:10.1021/ja502759d).

99 B. M. Lindley, Q. J. Bruch, P. S. White, F. Hasanayn and A. J. M. Miller, *J. Am. Chem. Soc.*, 2017, **139**, 5305-5308 (DOI:10.1021/jacs.7b01323).

100 A. Magistrato, A. Robertazzi and P. Carloni, *J. Chem. Theor. Comput.*, 2007, **3**, 1708-1720 (DOI:10.1021/ct700094y).